ORIGINAL RESEARCH

Transforming Growth Factor–induced Protein Promotes NF-κB–mediated Angiogenesis during Postnatal Lung Development

Min Liu[1], Cristiana Iosef[1], Shailaja Rao[1], Racquel Domingo-Gonzalez[1], Sha Fu[1,2], Paige Snider[3], Simon J. Conway[3], Gray S. Umbach[1,4], Sarah C. Heilshorn[5], Ruby E. Dewi[5], Mar J. Dahl[6], Donald M. Null[6], Kurt H. Albertine[6], and Cristina M. Alvira[1]

[1]Department of Pediatrics, Center for Excellence in Pulmonary Biology, and [5]Department of Materials Science and Engineering, Stanford University, Stanford, California; [2]Liuyang People's Hospital, Hunan, China; [3]Herman B Wells Center for Pediatric Research, Indiana University School of Medicine, Indianapolis, Indiana; [4]University of Texas Southwestern Medical School, Dallas, Texas; and [6]Department of Pediatrics, University of Utah School of Medicine, Salt Lake City, Utah

ORCID IDs: 0000-0002-9801-6304 (S.C.H.); 0000-0001-8497-0861 (K.H.A.); 0000-0002-6921-0001 (C.M.A.).

Abstract

Pulmonary angiogenesis is a key driver of alveolarization. Our prior studies showed that NF-κB promotes pulmonary angiogenesis during early alveolarization. However, the mechanisms regulating temporal-specific NF-κB activation in the pulmonary vasculature are unknown. To identify mechanisms that activate proangiogenic NF-κB signaling in the developing pulmonary vasculature, proteomic analysis of the lung secretome was performed using two-dimensional difference gel electrophoresis. NF-κB activation and angiogenic function was assessed in primary pulmonary endothelial cells (PECs) and TGFBI (transforming growth factor-β–induced protein)–regulated genes identified using RNA sequencing. Alveolarization and pulmonary angiogenesis was assessed in wild-type and *Tgfbi* null mice exposed to normoxia or hyperoxia. Lung TGFBI expression was determined in premature lambs supported by invasive and noninvasive respiratory support. Secreted factors from the early alveolar, but not the late alveolar or adult lung, promoted proliferation and migration in quiescent, adult PECs. Proteomic analysis identified TGFBI as one protein highly expressed by the early alveolar lung that promoted PEC migration by activating NF-κB via αvβ3 integrins. RNA sequencing identified *Csf3* as a TGFBI-regulated gene that enhances nitric oxide production in PECs. Loss of TGFBI in mice exaggerated the impaired pulmonary angiogenesis induced by chronic hyperoxia, and TGFBI expression was disrupted in premature lambs with impaired alveolarization. Our studies identify TGFBI as a developmentally regulated protein that promotes NF-κB–mediated angiogenesis during early alveolarization by enhancing nitric oxide production. We speculate that dysregulation of TGFBI expression may contribute to diseases marked by impaired alveolar and vascular growth.

Keywords: alveolarization; endothelial migration; colony-stimulating factor-3; nitric oxide production; bronchopulmonary dysplasia

In contrast to many organs, significant lung development occurs postnatally. During alveolarization, the final stage of lung development, division of primitive airspaces by secondary septation and exponential growth of the pulmonary microvasculature by angiogenesis markedly increases gas exchange surface area (1). Angiogenesis is a key driver of alveolarization. Inhibiting angiogenesis impairs alveolarization, whereas enhancing angiogenesis preserves alveolarization during injury (2, 3). Dysregulated angiogenesis is observed in premature infants with bronchopulmonary dysplasia (BPD), a chronic lung disease

(Received in original form April 21, 2020; accepted in final form October 29, 2020)

Supported by U.S. National Institutes of Health grants HL122918 (C.M.A.), HL148165 (S.J.C.), and HL110002 (K.H.A.), the Stanford Maternal Child Health Institute, the Tashia and John Morgridge Faculty Scholar Award (C.M.A.), the Stanford Chemical Engineering Undergraduate Summer Research Program (G.S.U.), the Stanford C.J. Huang SAMSUNG Fellowship (S.F.), and the University of Utah School of Medicine, Division of Neonatology (K.H.A.).

Author Contributions: M.L., C.I., S.R., R.D.-G., S.F., G.S.U., S.C.H., R.E.D., and C.M.A. designed and executed studies and analyzed and interpreted results. P.S. and S.J.C. created the *Tgfbi* null mice. M.J.D., D.M.N., and K.H.A. designed and executed the studies on preterm lambs. M.L. and C.M.A. drafted the manuscript. All authors contributed significant edits, gave final approval for publication, and agree to be accountable for the integrity of the information contained in this manuscript.

Correspondence and requests for reprints should be addressed to Cristina M. Alvira, M.D., Department of Pediatrics, Center for Excellence in Pulmonary Biology, Stanford University School of Medicine, 770 Welch Road, Suite 435, Palo Alto, CA 94304. E-mail: calvira@stanford.edu.

This article has a related editorial.

This article has a data supplement, which is accessible from this issue's table of contents at www.atsjournals.org.

Am J Respir Cell Mol Biol Vol 64, Iss 3, pp 318–330, Mar 2021

Originally Published in Press as DOI: 10.1165/rcmb.2020-0153OC on December 2, 2020
Internet address: www.atsjournals.org

Clinical Relevance

Our data identified a novel pathway of myofibroblast–endothelial cross-talk mediated through TGFBI (transforming growth factor-β–induced protein) that serves as a key mechanism that drives the rapid pulmonary angiogenesis that occurs at early alveolarization. We believe that this work has important implications for lung development, injury, and repair across the entire lifespan. By identifying and carefully characterizing a novel pathway, this work addresses both fundamental biology and putative therapeutic targets for investigators engaged in lung, vascular, and regenerative medicine.

characterized by impaired alveolarization that represents the most common complication of extreme prematurity (4). The extension of alveolarization into postnatal life provides an important window of opportunity for lung repair and regeneration (5). Thus, elucidating pathways that promote pulmonary angiogenesis and alveolarization has important clinical implications.

We previously showed that endogenous NF-κB activation promotes pulmonary angiogenesis in the early alveolar lung (6). Blocking NF-κB in early alveolar pulmonary endothelial cells (PECs) impairs angiogenic function, and pharmacologic inhibition of NF-κB in young mice impairs alveolar and vascular growth yet has no effect on adult mice. However, the mechanisms that induce temporal-specific activation of NF-κB in the developing pulmonary vasculature remain unknown.

The tissue microenvironment modulates angiogenesis in development and disease. During early lung development, the alveolar epithelium regulates vascular patterning by expressing VEGF (vascular endothelial growth factor) to promote EC survival, proliferation, and migration. In cancer, activated stromal fibroblasts develop a myofibroblast phenotype, colocalize with tumor vasculature, and promote angiogenesis by expressing growth factors and modulating the extracellular matrix (7). Although myofibroblasts are required for alveolarization (8), whether they function to regulate pulmonary angiogenesis has not been explored.

In this study, we hypothesized that unique factors in the early alveolar microenvironment induce temporal-specific activation of NF-κB in the pulmonary endothelium. We profiled the lung secretome during development and identified TGFBI (transforming growth factor-β–induced protein) as protein highly expressed by myofibroblasts during early alveolarization. We show that TGFBI induces NF-κB activation through αvβ3 integrins, increasing nitric oxide (NO) production by increasing the expression of *Csf3* (colony-stimulating factor-3), an NF-κB downstream target gene. *Tgfbi* null mice exhibit decreased pulmonary vascular density and a marked impairment of alveolar and vascular growth in response to chronic hyperoxia. Further, TGFBI expression was dysregulated in a premature lamb model of disrupted alveolarization. Together, our data identify a novel myofibroblast–endothelial cell axis that serves to guide pulmonary angiogenesis during early alveolarization and implicate a role for dysregulated TGFBI in the pathogenesis of BPD.

Some of the results of these studies have been previously reported in preprint form (https://doi.org/10.1101/2020.05.28.121871).

Methods

Please *see* the data supplement for full details.

Animal Models

C57BL/6 neonatal mice at early alveolarization (P6) and adult mice were purchased from Charles River Lab. *Tgfbi* null ($Tgfbi^{-/-}$) mice have been described previously (9). Mice containing an endothelial cell–specific deletion of *Ikkβ* were generated by crossing $Ikk\beta^{fl/fl}$ mice (10) with *Pdgfb-iCre* mice (11). For hyperoxia experiments, litters of P0 pups were maintained in room air (normoxia) or 80% O_2 (hyperoxia) for 14 days (12). Lung morphometric analysis was performed as previously described (6, 13).

The methods for delivery and management of chronically ventilating preterm lambs are reported (14–17). Time-pregnant ewes at 132 ± 2 days of gestation (term ~150 d gestation) were used. At ~3 hours of age, the preterm lambs were randomized to invasive mechanical ventilation (IMV) or noninvasive respiratory support (NRS), as previously described (16), for a total of 21 days. Control lambs were born at term.

Protocols for the animal studies adhered to American Physiological Society/National Institutes of Health guidelines for humane use of animals for research and were prospectively approved by the Institutional Animal Care and Use Committee at Stanford University and the University of Utah Health Sciences Center.

Lung Conditioned Media

Lung conditioned media (LCM) was prepared from lung tissue from C5BL/6 mice at the early alveolar (P6), late alveolar (P16), and adult (8–10 wk) stages of development (18), and proteins were analyzed by two-dimensional difference gel electrophoresis (2D DIGE) protein expression profiling.

Western Immunoblot and Immunofluorescence

Whole cell protein lysates were extracted from lung tissue and Western blot performed (13). Immunostaining was performed on formalin-fixed or frozen lung sections (6), probed with primary antibodies against CD31, TGFBI, NF-κB p65, or von Willebrand factor.

Isolation of Primary PECs

PECs were isolated from P6 or adult C57BL/6, $Tgfbi^{-/-}$ and $Tgfbi^{+/+}$, and *Pdgfb*-iCre$^{-/-}$$Ikk\beta^{fl/fl}$ and *Pdgfb*-iCre$^{+/-}$$Ikk\beta^{fl/fl}$ mice as described previously (6, 13). PEC isolation by this method with CD31 magnetic beads were ~95% pure based on staining for additional EC markers such as CD102 (8). Cells from passage 0 to 2 were used for all assays as described in the data supplement. TGFBI neutralization was performed with anti-TGFBI antibodies (4 μg/ml) and TGFBI stimulation with recombinant TGFBI (10 μg/ml) (19). NF-κB inhibition was performed with the pharmacologic inhibitor BAY 11-0782 (2.5 μM) and αvβ3 inhibition with signaling anti-αvβ3 integrin (4 μg/ml) antibodies.

RNA Interference

PECs were transfected with nontargeting control (NTC), integrin αV, integrin β3, or

Csf3 On-Target Plus SMART pool siRNA using Lipofectamine 2000 for 6 hours as previously described (20).

Multiplex Fluorescent *In Situ* Hybridization

PECs from P6 *Pdgfb-Cre*$^{+}$*Ikkβ*$^{fl/fl}$ and *Pdgfb-Cre*$^{-}$*Ikkβ*$^{fl/fl}$ mice were treated with 4-OHT and stimulated with TGFBI; colocalization of *Csf3* and PEC marker *Pecam1* were detected in PECs using RNAscope *in situ* hybridization per the manufacturer's protocol (ACD).

RNA-Sequencing Analysis

Total RNA was extracted and RNA sequencing (RNA-seq) performed by Quick Biology. Genes showing altered expression with $P < 0.05$ and more than 1.5-fold change were considered differentially expressed.

Measurement of NO in PECs

NO production was determined by loading the cells with 4-amino-5-methylamino-2′,7′-difluorofluorescein diacetate before immunofluorescent imaging as previously described (21).

Statistics

Statistical differences between two groups were determined by Student's *t* test or one- or two-way ANOVA as appropriate. A *P* value of ⩽0.05 was considered statistically significant.

Results

Factors Secreted by the Early Alveolar Lung Activate Proangiogenic Pathways in Adult PECs

To determine if factors present in the early alveolar microenvironment activate NF-κB and modulate PEC angiogenic function, we collected LCM from mice at different stages of development and assessed NF-κB activation and PEC migration. Under control conditions, NF-κB subunits are constitutively expressed but only translocate to the nucleus upon activation. At baseline, adult PECs demonstrated minimal active NF-κB (Figure 1A). However, incubation with early alveolar LCM increased NF-κB activation by 2.65-fold ($P < 0.001$) (Figures 1A and 1B). In contrast, incubation with late alveolar LCM increased NF-κB activation only slightly ($P < 0.05$), and adult LCM had no effect. Similarly, adult PECs migrated slowly when cultured in starvation media (Figure 1C). The early alveolar LCM was as effective as 5% FBS in inducing adult PEC migration, resulting in 43% scratch closure ($P < 0.0001$). In contrast, the adult LCM induced migration only minimally ($P < 0.05$). Taken together, these data suggested that factors present in the early alveolar lung microenvironment can induce NF-κB activation and promote migration in adult PECs.

TGFBI Is Highly Expressed in the Early Alveolar Lung but Absent in the Adult Lung

To identify factors uniquely present in the early alveolar lung microenvironment, we compared all of the secreted proteins in the three LCM by 2-D DIGE (Figure E1 in the data supplement), and identified 20 proteins that were highly expressed in the early alveolar lung secretome by mass spectrometry (Table E1). Of this group, we selected TGFBI for further investigation, a classically secreted protein that has recently been shown to be highly expressed by myofibroblasts by single-cell RNA-seq of the developing mouse lung (22). We confirmed higher expression of TGFBI in the early alveolar LCM ($P < 0.001$, Figure 2A), and in agreement with previous data (9), highest TGFBI protein in whole lung during early alveolarization, followed by an age-dependent decrease over time (Figure 2B). Immunostaining of early alveolar lung tissue identified numerous cells with intense TGFBI expression (Figure 2C), located at the tips of secondary septa, characteristic locations for alveolar myofibroblasts. In contrast, TGFBI immunoreactivity was completely absent in the adult lung. Similar findings were observed in the lungs of lambs (Figure 2D), with high

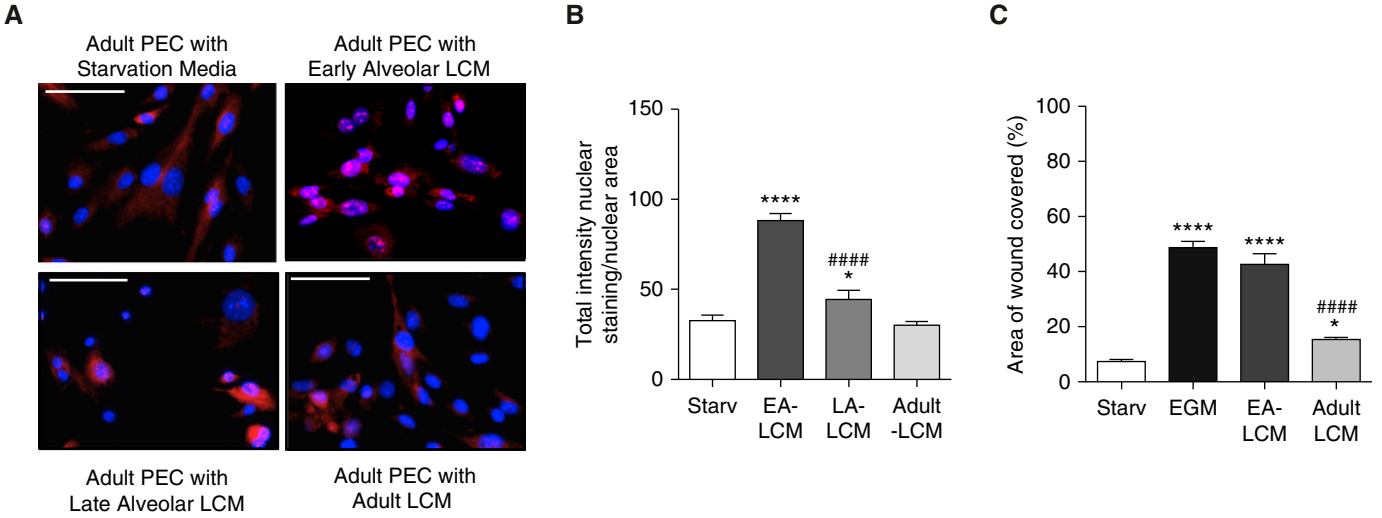

Figure 1. Factors secreted by the early alveolar lung activate proangiogenic pathways in adult PECs. (*A*) Representative immunofluorescent images of adult PECs incubated with starvation media or early alveolar (EA), late alveolar, or adult LCM for 24 hours followed by immunostaining to detect the NF-κB subunit, p65 (red) and chromatin (blue). Scale bars, 50 μm. (*B*) Quantification of the total intensity of nuclear p65 with $^{*}P < 0.05$ and $^{****}P < 0.0001$ versus starvation, and $^{\#\#\#\#}P < 0.0001$ versus EA-LCM, with $n = 6$ per group. (*C*) EC scratch assays performed using adult PECs incubated with starvation media, 5% FBS, EA-LCM, and adult LCM, and the percent scratch area covered at 24 hours calculated. $^{*}P < 0.05$ and $^{****}P < 0.0001$ versus starvation, and $^{\#\#\#\#}P < 0.0001$ versus EA-LCM, with $n = 3$ per group. LA = late alveolar; LCM = lung conditioned media; PEC = pulmonary endothelial cells; Starv = starvation media.

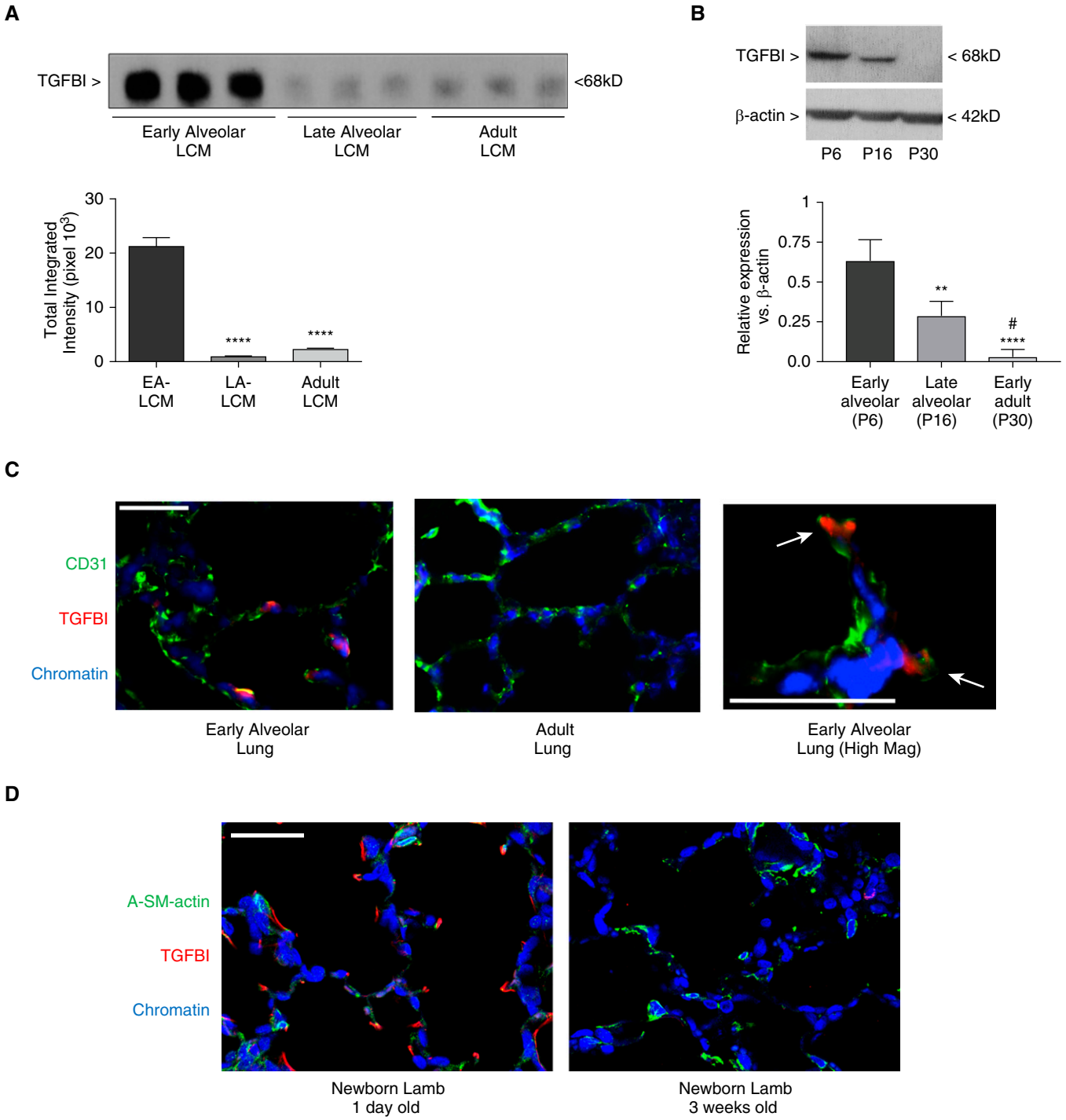

Figure 2. TGFBI (transforming growth factor-β–induced protein) is highly expressed in the early alveolar lung but absent in the adult lung. (*A*) Western blot to determine TGFBI protein in the EA-, LA-, and adult LCM. $^{****}P < 0.0001$ versus EA = LCM, with $n = 3$. (*B*) Western blot to determine TGFBI protein relative to β-actin in whole lung from mice at the early alveolar (P6), late alveolar (P16), and adult (P30) stages of development. $^{**}P < 0.01$ and $^{****}P < 0.0001$ versus P6, and $^{\#}P < 0.05$ versus P16, with $n = 4$ per group. (*C*) Representative images obtained from lung cryosections obtained from P6 and adult mice to detect CD31 (green), TGFBI (red), and chromatin (blue). Arrows point to TGFBI-positive cells at tips of secondary septa. Scale bars, 100 μm. (*D*) Representative images obtained from lung tissue from lambs at the early alveolar (Day 1) and late alveolar (3 wk) stages of development to detect ACTA2 (green), TGFBI (red), and chromatin (blue). Scale bar, 50 μm. Mag = magnification.

TGFBI expression in cells at the septal tips at 1 day of life, corresponding to early alveolarization, but reduced TGFBI expression by 3 weeks of age.

TGFBI Is Necessary and Sufficient for Promoting Early Alveolar and Adult PEC Migration

We next determined whether TGFBI was required for the early alveolar LCM to enhance adult PEC migration. The addition of anti-TGFBI antibodies, but not isotype control IgG, significantly impaired, but did not completely abrogate, the capacity of the early alveolar LCM to promote adult PEC migration ($P < 0.0001$, Figure 3A) but had no effect on its proliferative effect (Figure 3B). To determine whether TGFBI was sufficient to promote PEC migration, we used recombinant TGFBI (rTGFBI) in microfluidic chemotaxis assays that permitted the creation of stable, linear gradients of chemotactic agents. Early alveolar PECs exposed to a gradient of starvation media migrated randomly, whereas those exposed to a gradient of VEGF demonstrated directed migration toward the source ($P < 0.0001$) (Figure 3C). Both the early alveolar LCM and rTGFBI induced similar directed migration, although VEGF was a more potent

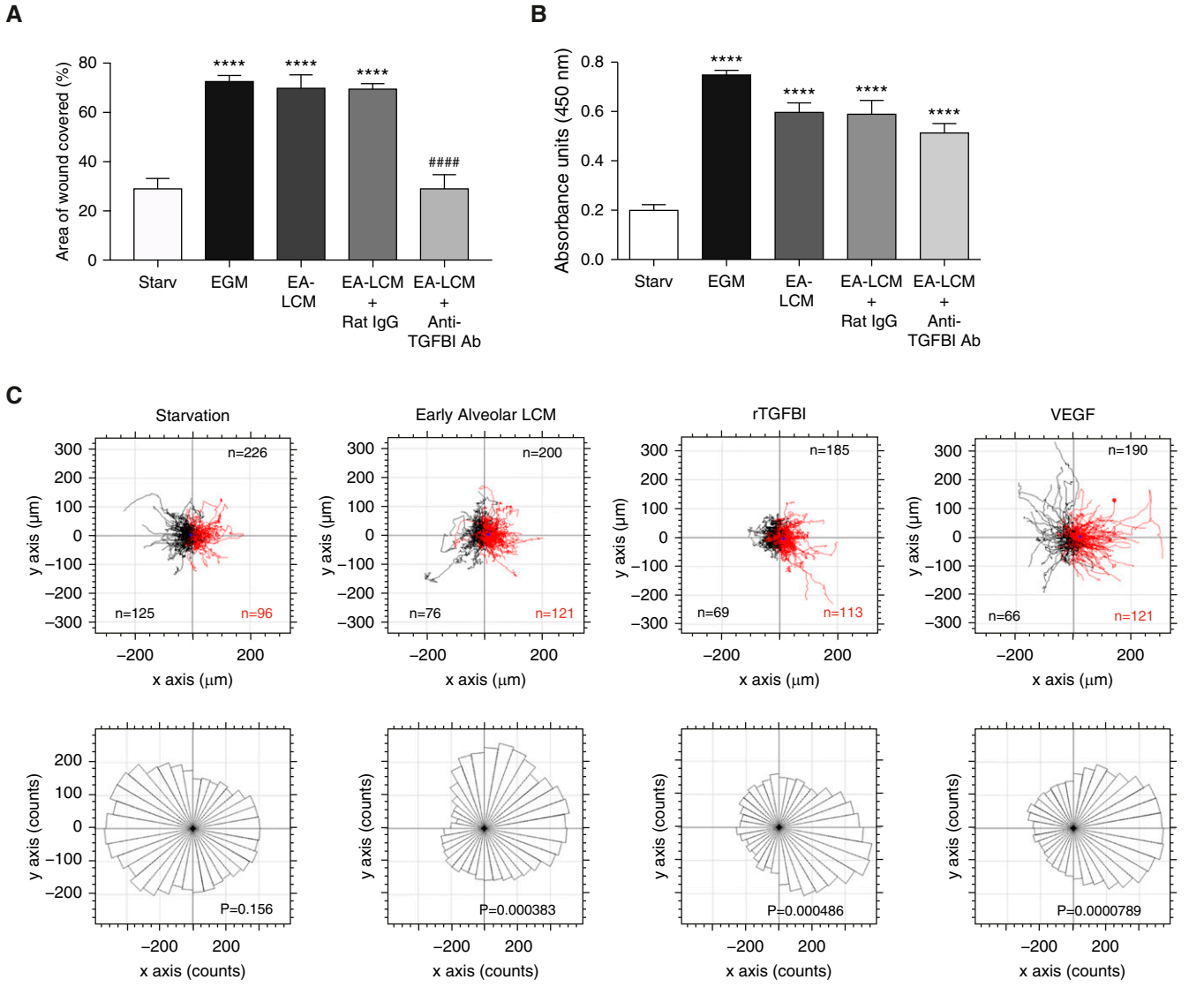

Figure 3. TGFBI is necessary and sufficient to promote PEC migration. (*A*) Endothelial scratch assays were performed using adult PECs incubated with starvation media, 5% FBS, EA-LCM, EA-LCM plus isotype control IgG, and EA-LCM plus anti-TGFBI antibodies (4 μg/ml) and the percent scratch area covered at 24 hours calculated. $^{****}P < 0.0001$ versus starvation, and $^{\#\#\#\#}P < 0.0001$ versus EA-LCM, with $n = 3$ per group. Representative results from three separate experiments. (*B*) BrdU incorporation assays to assess adult PEC proliferation at 24 hours in cells incubated with 5% FBS, EA-LCM, EA-LCM + IgG, and EA-LCM + anti-TGFBI antibodies. $^{****}P < 0.0001$ versus starvation with $n = 3$–6 per group. (*C*) Tracks of individual cells (top) and directional histograms (bottom) from live cell imaging and tracking of early alveolar PECs subjected to microfluidic chemotaxis assays performed with starvation media, EA-LCM, starvation + TGFBI, or starvation + VEGF (50 ng/ml) with each chamber containing a source on the right side and a sink on the left. Total number of individual cells tracked is reported in the upper left corner, and the number of cells migrating away (black) or toward (red) in the bottom left and right corners, respectively. In each group there were between three and five cells with a migration of net zero, accounting for the remaining cells making up the total number. *P* value is shown on the image. Ab = antibody; rTGFBI = recombinant TGFBI; VEGF = vascular endothelial growth factor.

chemoattractant as it was able to stimulate migration at much lower doses. Moreover, rTGFBI promoted migration of both the early alveolar and adult PECs in endothelial scratch assays and Boyden chamber assays (Figure E2).

TGFBI-mediated PEC Migration Is NF-κB Dependent

We next assessed whether the promigratory effect of TGFBI is NF-κB dependent. Similar to the migration results, early alveolar LCM containing control IgG increased NF-κB activation by 80% ($P < 0.001$), but the addition of anti-TGFBI antibodies significantly blunted this effect ($P < 0.05$) (Figure 4A). rTGFBI significantly increased NF-κB activity in early alveolar PECs (Figure 4B, $P < 0.001$),

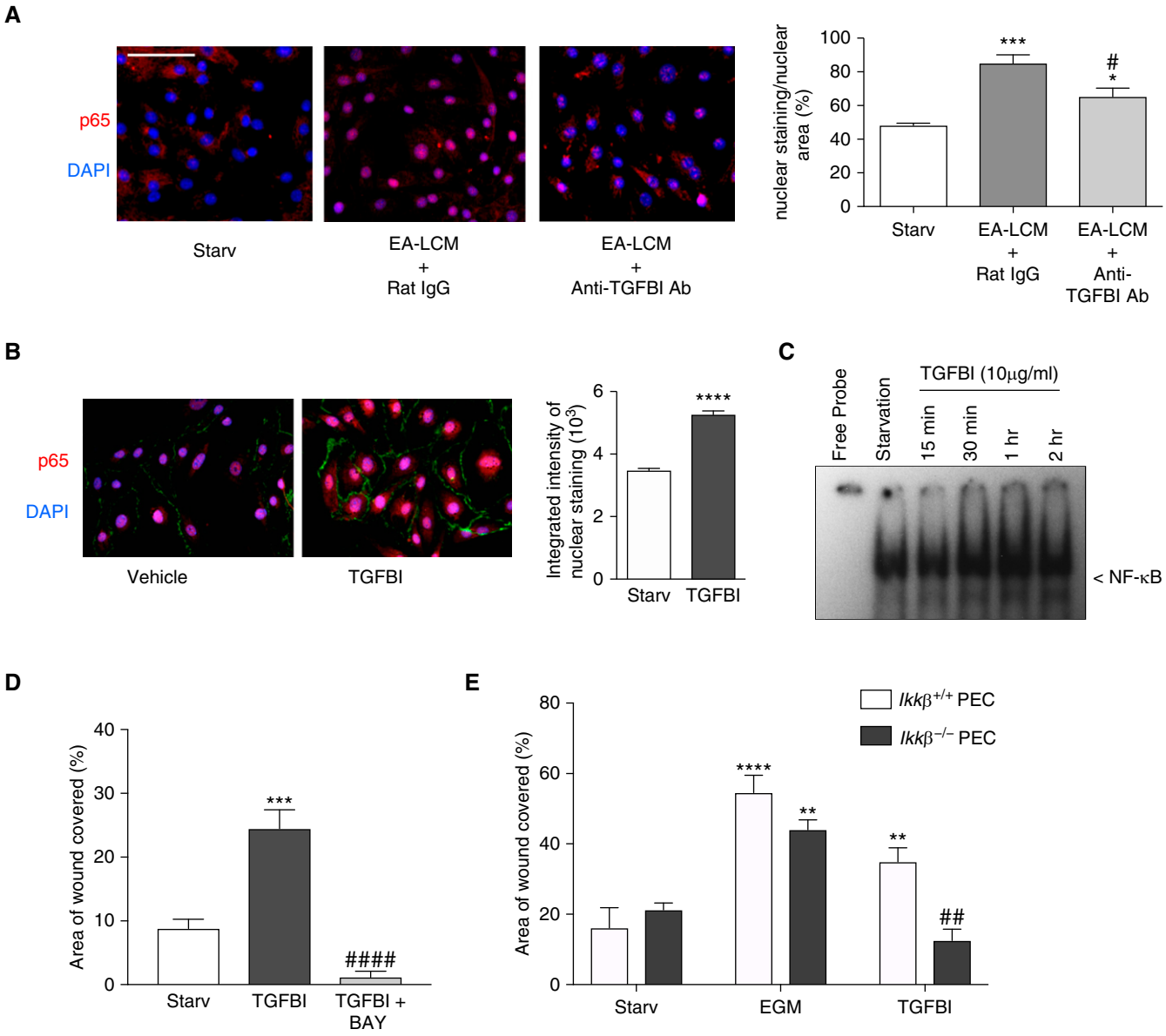

Figure 4. TGFBI-mediated pulmonary endothelial cell migration is NF-κB dependent. (*A*) Representative images of adult PECs incubated with starvation media, EA-LCM + IgG, and EA-LCM + anti-TGFBI antibodies for 24 hours followed by immunostaining to detect p65 (red) and chromatin (blue), with quantification to determine the total intensity of nuclear p65 over nuclear area. $^{*}P < 0.05$ and $^{***}P < 0.001$ versus starvation, and $^{\#}P < 0.05$ versus EA-LCM + IgG, with $n = 5$ per group. Scale bar, 50 μm. (*B*) Representative images from early alveolar PECs incubated with starvation media + vehicle or starvation media + rTGFBI for 24 hours stained to detect the p65 (red), CD31 (green), and DAPI (blue), with quantification of total intensity of nuclear p65. $^{****}P < 0.0001$ with $n = 127$ control cells and $n = 112$ rTGFBI-stimulated cells. (*C*) Representative electrophoretic mobility shift assay to detect NF-κB–DNA binding in early alveolar PECs exposed to starvation media or starvation media + TGFBI. (*D*) Scratch assays using early alveolar PECs stimulated with starvation media, starvation media + rTGFBI, or starvation media + rTGFBI and BAY 11-7082 (2.5 μM), with the percent scratch area covered at 24 hours calculated. $^{***}P < 0.001$ versus starvation and $^{\#\#\#\#}P < 0.0001$ versus rTGFBI, with $n = 4$ per group. (*E*) Scratch assays performed using wild-type PECs ($Ikk\beta^{+/+}$) and PECs lacking the NF-κB activator, IKKβ ($Ikk\beta^{-/-}$) stimulated with starvation media, EGM, starvation media + rTGFBI, and the percent scratch area covered at 24 hours calculated. $^{**}P < 0.01$ and $^{****}P < 0.0001$ versus starvation, and $^{\#\#}P < 0.01$ versus TGFBI-treated $Ikk\beta^{+/+}$ PECs, with $n = 4$ per group. BAY = BAY-7082; EGM = endothelial growth media.

and increased NF-κB–DNA binding as early as 30 minutes, with peak NF-κB–DNA binding observed at 1 hour (Figure 4C). In addition, inhibiting NF-κB with BAY-7082 (23) completely abrogated TGBFI-mediated migration ($P < 0.0001$, Figure 4D). Furthermore, we performed studies using PECs obtained from mice containing an endothelial-specific deletion of *Ikkβ*, the primary activator of NF-κB in early alveolar PECs (20). Although rTGFBI increased migration in wild-type (WT) PECs ($P < 0.01$), TGFBI-induced migration was absent in PECs lacking *Ikkβ*. Taken together, these data demonstrate that TGFBI-mediated migration is IKKβ/NF-κB dependent (Figure 4E).

TGFBI-mediated NF-κB Activation and Endothelial Migration Requires avβ3 Integrins

We next performed studies to identify how TGFBI was mediating these effects. TGFBI contains a carboxy-terminal Arg-Gly-Asp (RGD) sequence that allows binding to integrins (24). We focused initially on αvβ3, an integrin upregulated in angiogenic vascular tissue (25) that activates NF-κB in ECs (26, 27). rTGFBI significantly increased NFκB activity in early alveolar PECs pretreated with control IgG but had no effect on PECs treated with anti-αvβ3 integrin antibodies (Figures 5A and 5B). Although both rTGFBI alone and rTGFBI + IgG promoted PEC migration to a similar degree (Figure 5C), anti-αvβ3 antibodies completely blocked rTGFBI-induced PEC migration. Finally, we transfected early alveolar PECs with NTC, αv integrin, or β3 integrin siRNA. In vehicle-stimulated cells, migration was similar between the three groups (Figure 5D). rTGFBI significantly increased migration in the NTC-transfected PECs ($P < 0.01$) but did not increase migration in PECs transfected with either αv or β3 siRNA.

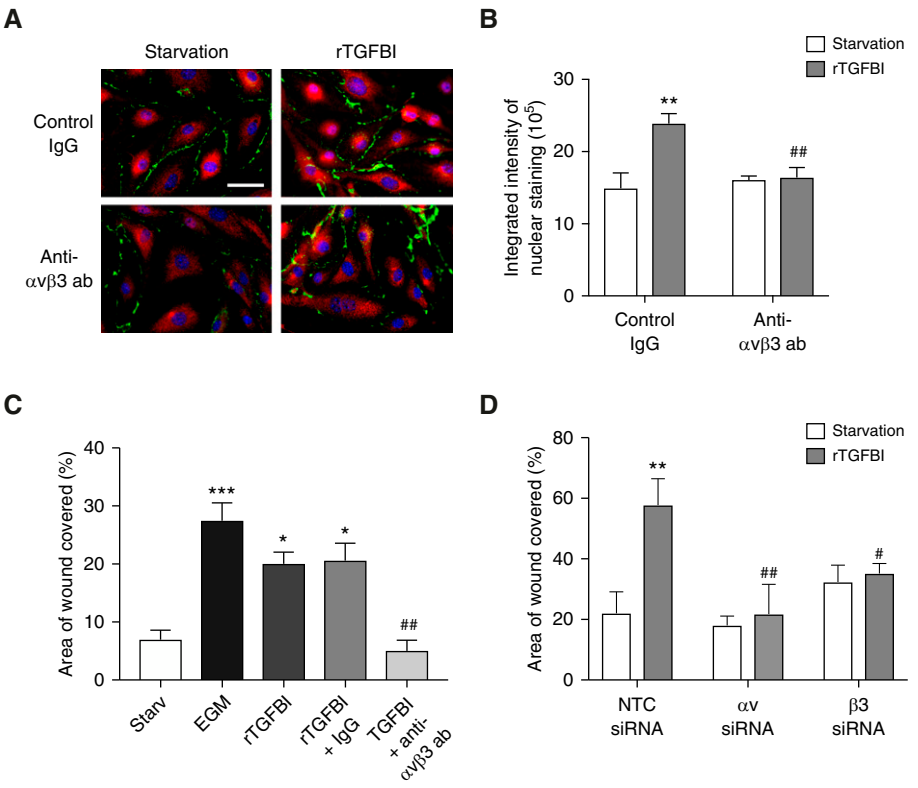

Figure 5. TGFBI–mediated endothelial migration requires αvβ3 integrins. (*A*) Representative images obtained from early alveolar PECs pretreated with either IgG or anti-αvβ3 antibodies before stimulation with starvation media + vehicle or starvation media + rTGFBI for 24 hours stained to detect the p65 (red), CD31 (green), and DAPI (blue), with (*B*) quantification of total intensity of nuclear p65. Scale bar, 20 μm. $^{**}P < 0.01$ versus starvation + IgG, and ## versus rTGFBI + IgG with $n = 4$. (*C*) Scratch assays with early alveolar PECs incubated with starvation media, EGM, starvation media + rTGFBI, starvation media + rTGFBI + IgG, and starvation media + rTGFBI plus anti-αvβ3 antibodies and the percent scratch area covered at 24 hours calculated. $^{*}P < 0.05$ and $^{***}P < 0.001$ versus starvation, and $^{\#\#}P < 0.01$ versus starvation + rTGFBI + IgG, with $n = 3$ per group. Representative result from two independent experiments. (*D*) Scratch assays were performed using early alveolar PECs transfected with nontargeting control (NTC), integrin αv, and integrin β3 siRNA. At 48 hours after transfection, the groups were incubated with starvation media, EGM, and starvation media + rTGFBI and the percent scratch area covered at 24 hours calculated. $^{**}P < 0.01$ versus starvation, and $^{\#}P < 0.05$ and $^{\#\#}P < 0.01$ versus NTC stimulated with rTGFBI, with $n = 3$–4 per group. Representative result from four independent experiments.

TGFBI Promotes Migration of Early Alveolar PECs by Increasing NF-κB–mediated Csf3 Expression to Enhance NO Production

To identify mechanism by which TGFBI promotes PEC migration, we profiled TGFBI-responsive genes using RNA-seq. Given that rTGFBI stimulated both early alveolar and adult PEC migration (Figure E2), we looked for genes induced by rTGFBI in both groups. Hierarchical clustering of differentially expressed genes demonstrated good clustering of vehicle- and rTGFBI-stimulated samples (Figure 6A). rTGFBI significantly dysregulated 56 genes in early alveolar (Table E2) and 64 genes in adult PECs (Table E3); however, only three genes were shared (Figure E3A). *Csf3*, a known NF-κB target gene, was among the shared genes, upregulated 3.01-fold in early alveolar and 2.77-fold in adult PECs by rTGFBI (Figure E3B). We confirmed that rTGFBI induced a 3.4-fold increase in *Csf3* gene expression in early alveolar PECs ($P < 0.05$) by quantitative PCR (Figure 6B), and increased CSF3 protein ($P < 0.01$) (Figure 6C). To determine if *Csf3* expression in the PECs requires NF-κB activation, we performed multiplex *in situ* hybridization to simultaneously detect *Csf3* and *Pecam1* in $Ikk\beta^{+/+}$ and $Ikk\beta^{-/-}$ PECs isolated from P6 pups. Using this method, we conformed that *Csf3* is expressed in *Pecam1*-positive cells (Figure 6D). rTGFBI stimulation for 4 hours increased *Csf3* expression by 2.7-fold in $Ikk\beta^{+/+}$ PECs ($P < 0.0001$) but failed to increase *Csf3* expression in the $Ikk\beta^{-/-}$ PECs (Figure 6D).

Prior studies found that CSF3 promotes EC migration by increasing in NO (28). Therefore, we next loaded cells with the NO-sensitive dye

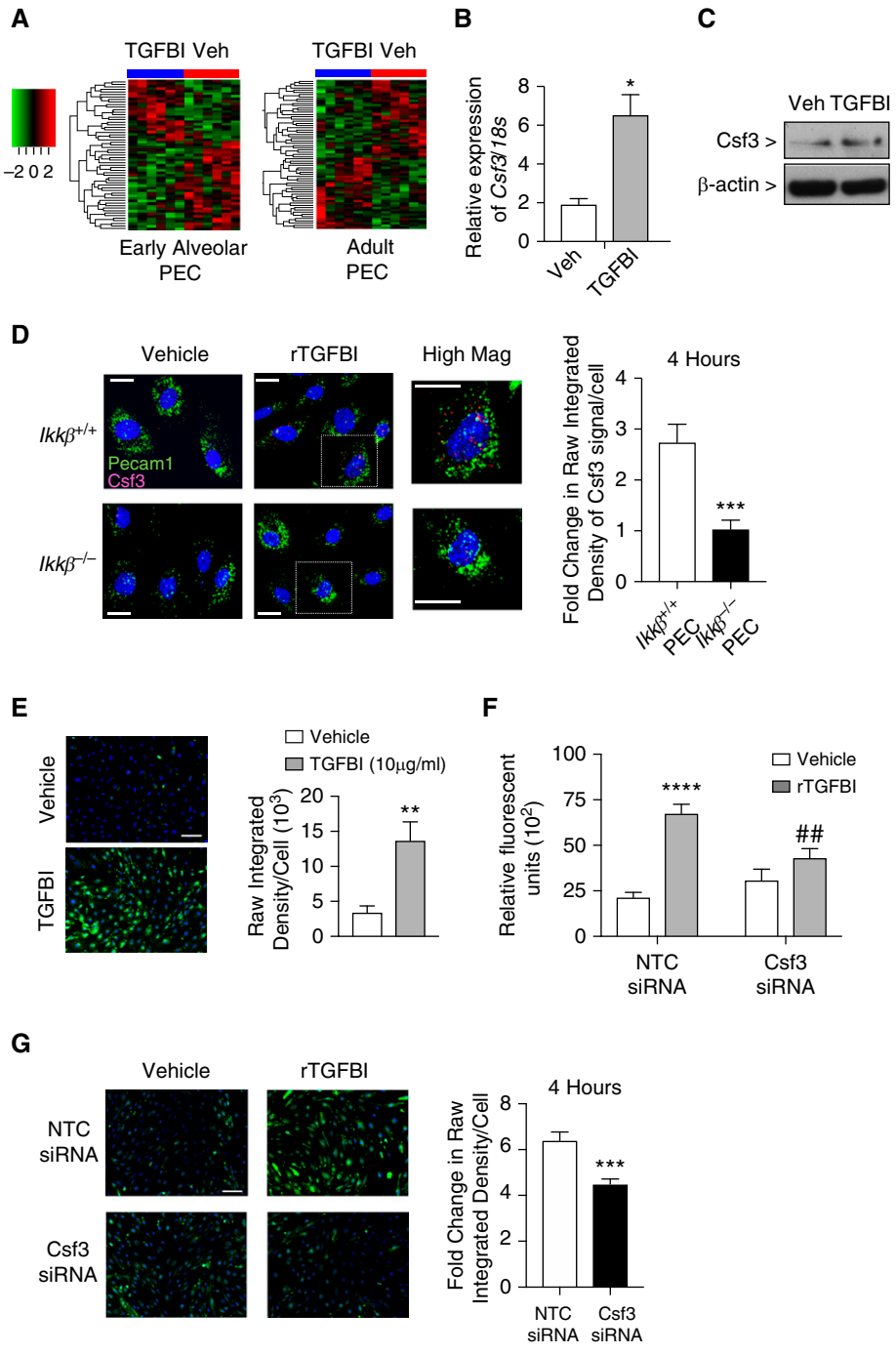

Figure 6. TGFBI induces an NF-κB–dependent expression of Csf3 (colony-stimulating factor-3), a modulator of nitric oxide (NO), in early alveolar PECs. (*A*) Heat map of differentially expressed genes identified by RNA sequencing in early alveolar and adult PECs stimulated with vehicle or rTGFBI for 6 hours. Upregulated genes are in red and downregulated genes in green. (*B*) Gene expression of Csf3 was determined by qRT-PCR in early alveolar PECs stimulated with vehicle or rTGFBI for 6 hours. $^{*}P < 0.05$ versus vehicle with $n = 4$ per group. (*C*) Representative Western blot to detect CSF3 protein expression in whole cell lysates obtained from early alveolar PECs stimulated with vehicle or rTGFBI for 4 hours. (*D*) Representative *in situ* hybridization images to detect Csf3 (red) and Pecam1 (green) in *Ikkβ*$^{+/+}$ and *Ikkβ*$^{-/-}$ PECs treated with vehicle or rTGFBI for 4 hours, with quantification of the fold change in raw integrated density of Csf3 mRNA particles per cell compared with vehicle. Scale bar, 20 μm. $^{***}P = 0.0006$ versus *Ikkβ*$^{+/+}$ PEC. (*E*) NO production assays in early alveolar PECs stimulated with starvation media containing vehicle or rTGFBI for 4 hours and loaded with the 4-amino-5-methylamino-2′,7′-difluorofluorescein diacetate before stimulation with vehicle or rTGFBI and found that rTGFBI increased NO in the PECs by more than twofold compared with vehicle at 4 and 24 hours (Figures 6E and E3D). To determine if the TGFBI-mediated effects require *Csf3*, we performed additional studies where we silenced *Csf3*. Transfection of early alveolar PECs with *Csf3* siRNA effectively reduced CSF3 protein expression by 42 hours (Figure E3C). Incubation of NTC siRNA-transfected cells with rTGFBI for 8 hours increased migration twofold ($P < 0.0001$) (Figure 6F) but did not significantly enhance migration in *Csf3* siRNA-transfected cells. rTGFBI also enhanced NO production in NTC siRNA-transfected cells (Figure 6G). However, rTGFBI-mediated increases in NO were significantly decreased with *Csf3* silencing. Taken together, these results demonstrate that TGFBI promotes PEC migration by augmenting NF-κB–mediated *Csf3* expression to increase NO production.

Loss of TGFBI Impairs Pulmonary Vascular Growth in Mice, and TGFBI Expression Is Dysregulated in Preterm Lambs with Impaired Alveolarization

To assess the physiological role of TGFBI in alveolarization and pulmonary angiogenesis, we evaluated mice containing a global deletion of TGFBI in normoxia and in response to chronic hyperoxia, a stimulus that disrupts pulmonary angiogenesis and alveolarization (29). These mice were reported to have impaired alveolarization at baseline, but abnormalities in vascular growth were not observed in that initial report. In keeping with prior results, *Tgfbi* null mice exhibited a 20% decrease in radial alveolar count ($P < 0.0001$) and a 128% increase in distal airspace area ($P < 0.0001$) compared with WT mice (Figures 7A–7C). As expected, chronic hyperoxia disrupted alveolarization in the WT mice but induced a more exaggerated phenotype in the *Tgfbi* null mice, reducing radial alveolar count by almost 70% ($P < 0.0001$), and further increased the already dilated distal airspaces ($P < 0.001$). Under control conditions, *Tgfbi* null mice exhibited a 33% reduction in pulmonary vascular density as compared with WT ($P < 0.0001$) (Figures 7D and 7E). Chronic hyperoxia reduced pulmonary vascular density in WT mice by 46%

($P < 0.0001$) but caused a more exaggerated disruption of pulmonary vascular growth in the *Tgfbi* null mice, decreasing pulmonary vascular density by 70% ($P < 0.0001$), resulting in an almost threefold reduction in distal vessels in *Tgfbi* null compared with WT mice. Taken together, these results demonstrate that TGFBI is required for physiologic pulmonary vascular growth and that loss of TGFBI worsens the detrimental effects of chronic hyperoxia on alveolarization and angiogenesis.

Finally, we explored whether TGFBI expression was altered in a large animal model of BPD, where preterm lambs are supported with either NRS or IMV. Control, term lambs had focal staining of TGFBI throughout the lung, including high expression at the tips of all the secondary septa (Figure 7F). Preterm lambs supported with NRS exhibited many thin secondary septa and a marked reduction in TGFBI immunostaining. Preterm lambs supported by IMV, however, had abnormally thickened secondary septa, with a heightened expression but abnormal localization of TGFBI along the length of the thick secondary septa rather than the normal localization at the septal tips.

Discussion

During early postnatal life, growth of the pulmonary vasculature serves as a driver of alveolarization. In this study, we explored the mechanisms that activate proangiogenic NF-κB signaling in the pulmonary endothelium during early alveolarization. We identified TGFBI as a secreted protein highly expressed by myofibroblasts in early alveolarization (22), corresponding to the time when NF-κB is endogenously active in the pulmonary vasculature (6). We show that TGFBI activates NF-κB in PECs and enhances NF-κB–mediated EC migration via αvβ3 integrins. We further show that TGFBI stimulation increases *Csf3* expression, serving to enhance NO production. Finally, we demonstrate that loss of TGFBI in mice impairs pulmonary vascular development at baseline and severely impairs alveolar and vascular growth in chronic hyperoxia, and that TGFBI expression and localization is aberrant in a preterm lamb model of disrupted alveolarization. In summary, our studies identify a novel axis, whereby developmental expression of TGFBI activates NF-κB and promotes pulmonary endothelial angiogenesis during this critical window of vascular development.

Pulmonary angiogenesis is essential for alveolarization, and disrupted angiogenesis contributes to the pathogenesis of BPD, the most common complication of premature birth (30). Our lab previously identified the NF-κB pathway as an important regulator of pulmonary angiogenesis during alveolarization (6). However, the mechanisms allowing for temporal-specific activation of proangiogenic NF-κB signaling in the pulmonary vasculature was not identified. These results highlight the role of paracrine factors secreted from alveolar myofibroblasts in the creation of a proangiogenic niche that activates NF-κB to support pulmonary vascular growth during early alveolarization.

By profiling developmental differences in the lung microenvironment, we identified TGFBI as a temporally regulated protein highly expressed during early alveolarization. However, the capacity of the EA-LCM to promote migration and activate NF-κB was not completely abrogated by the anti-TGFBI antibodies, suggesting that additional factors present in the early alveolar lung microenvironment also serve to enhance NF-κB–dependent proangiogenic signaling. TGFBI binds both extracellular matrix (31, 32) and integrins (33–35), suggesting a possible role as a bifunctional linker protein that connects cells to the matrix (31). TGFBI mRNA is biphasically altered in the hyperoxia mouse model of BPD (9) and induced during bleomycin-mediated fibrotic lung injury (36). Importantly, single-cell RNA-seq in the developing murine lung identified TGFBI as a highly discriminating gene for myofibroblasts (22). In our study, TGFBI was expressed at the tips of secondary crests, characteristic locations for myofibroblasts (8), concordant with a prior report that identified high expression of TGFBI in the septal tips of a 2 year-old child, leading the authors to speculate a putative role in alveolar morphogenesis (37).

In other systems, TGFBI is regulated by TGF-β. TGF-β isoforms play a complex role in lung development. Although TGF-β1 is expressed in the developing lung during branching morphogenesis (38), loss of TGF-β1 does not disrupt lung development (39). However, loss of TGF-β3 induces alveolar hypoplasia and extensive intrapulmonary hemorrhage, suggesting a role for TGF-β3 in pulmonary vasculature stabilization (40). Impaired alveolarization is also observed in mice with global deletions of Smad3, the downstream effector of TGF-β (41). Taken together, these data highlight the importance of precise TGF-β signaling in the correct cells at the right time to support lung development. Further studies will be needed to determine if TGF-β is the primary regulator of TGFBI in the early alveolar lung; however, as a putative downstream effector of TGF-β, our data highlight a role for TGFBI in coordinating alveolar and vascular growth during alveolarization.

TGFBI promotes cell adhesion, migration, and proliferation of diverse cell types by interacting via integrins (42). We specifically investigated αvβ3 integrins given their established role in angiogenesis. The αvβ3 integrin is highly expressed by newly forming blood vessels (25). Activation of αvβ3 promotes endothelial migration (43), and blocking αvβ3 inhibits tumor angiogenesis (44) and impairs lumen

Figure 6. (*Continued*). NO-sensitive dye 4-amino-5-methylamino-2′,7′-difluorofluorescein diacetate. Representative images were taken to detect NO (green) and chromatin (blue). Scale bar, 100 μm. Quantification of the raw integrated density of NO fluorescent signal per cell in early alveolar PECs stimulated with vehicle or rTGFBI for 4 hours, with $^{**}P < 0.01$ versus vehicle, with $n = 5$–8 per group. Results are representative of three independent experiments. (*F*) Boyden chamber assays to detect chemotactic migration in early alveolar PECs transfected with NTC or Csf3 siRNA incubated at 48 hours after transfection with starvation media or starvation media containing rTGFBI for 8 hours. $^{****}P < 0.0001$ versus vehicle and $^{\#\#}P < 0.01$ versus NTC siRNA transfected PECs treated with rTGFBI, with $n = 10$–12 replicates. Results are a representative example of three independent experiments. (*G*) NO production assays in early alveolar PECs transfected with NTC or Csf3 siRNA and stimulated with vehicle or rTGFBI for 4 hours. Representative images to detect NO (green) and chromatin (blue). Scale bar, 100 μm. Quantification of the fold change in raw integrated density of NO fluorescence per cell in NTC and Csf3 siRNA transfected PECs stimulated with rTGFBI compared with vehicle for 4 hours is shown. $^{***}P = 0.0008$ versus NTC transfected PECs. Veh = vehicle.

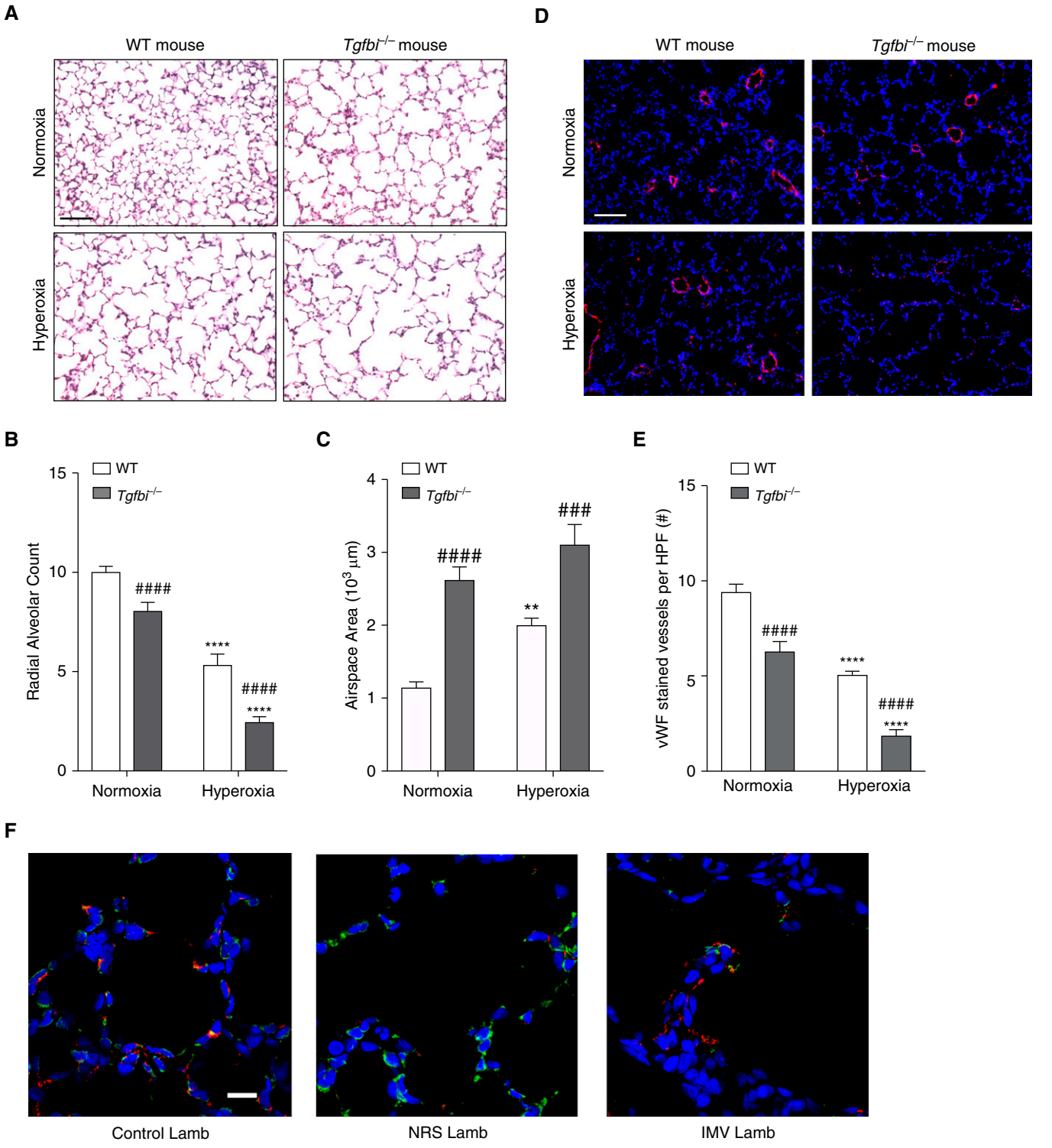

Figure 7. Loss of TGFBI in mice impairs pulmonary parenchymal and vascular growth and TGFBI expression is dysregulated in experimental models of impaired alveolarization. (*A*) Representative images obtained from P14 wild-type (WT) and *Tgfbi* null mice maintained in normoxia or chronic hyperoxia (80% O_2 from P1 to P14). Scale bar, 100 μm. Quantification of radial alveolar counts (*B* and *C*) distal airspace area. $^{**}P < 0.01$ and $^{****}P < 0.0001$ versus normoxia for each genotype, and $^{###}P < 0.001$ and $^{####}P < 0.0001$ versus WT via two-way ANOVA, with $n = 4$–7 per group. (*B*, *C*, and *E*) * denotes differences between normoxia and hyperoxia for each genotype, and # denotes differences between the genotypes in each condition. (*D*) Representative images stained to detect von Willebrand factor (vWF) (red) and DAPI (blue) in lungs taken from mice at P14. Scale bar, 100 μm. (*E*) Quantification of vWF-stained vessels <100 μm per high-powered field in 20 nonoverlapping sections per mouse. $^{****}P > 0.0001$ versus normoxia for each genotype, and $^{####}P < 0.0001$ versus WT with $n = 5$–7 mice per group. (*F*) Representative images obtained from control term newborn lambs, and premature lambs treated with noninvasive respiratory support or invasive mechanical ventilation, stained to detect TGFBI (red), ACTA2 (green), and chromatin (blue). Scale bar, 20 μm. IMV = invasive mechanical ventilation; NRS = noninvasive respiratory support.

formation and vascular patterning in the embryo (45). Furthermore, αvβ3 activates NF-κB to promote EC adhesion, survival, and migration (26, 46). Moreover, TGFBI promotes adhesion and migration of human umbilical ECs via αvβ3 (35). Concordant with these studies, we found that TGFBI-stimulated PEC migration was blocked by inhibiting either NFκB or αvβ3. Taken together, our data demonstrate that TGFBI promotes PEC migration via αvβ3 to induce proangiogenic NF-κB signaling.

We next investigated the downstream mechanisms by which TGFBI promotes PEC migration, using RNA-seq to identify novel TGFBI-regulated genes. One of the few shared targets in early alveolar and adult PECs was *Csf3* (encoding G-CSF), a known NF-κB target gene (47) that promotes endothelial migration (48). G-CSF increases the expression and activation of endothelial nitric oxide synthase (eNOS) to augment NO production (28). NO is produced locally at lamellipodia of migrating human EC, and lung EC from *eNOS* null mice migrate more slowly and display impaired capillary formation (49–51). In our study, TGFBI increased NO production in PECs, and silencing *Csf3* blocked both TGFBI-mediated NO production and PEC migration. Furthermore, rTGFBI failed to induce *Csf3* expression in $Ikk\beta^{-/-}$ PECs, demonstrating that the TGFBI-mediated *Csf3* upregulation requires NF-κB signaling. In preterm lambs, prolonged IMV reduced eNOS protein and pulmonary capillary and microvessel abundance (52, 53). Taken together, these studies identify *Csf3* as a central downstream mechanism for the proangiogenic effects of TGFBI.

Finally, as proof of concept for the importance of TGFBI *in vivo*, we performed studies using *Tgfbi* null mice and a preterm lamb model of impaired alveolarization (9, 16). Although a reduction in total von Willebrand factor positive vessels was not observed in the *Tgfbi* null mice at P7 in the original description of these mice, we found that by P14, there was a reduction in the density of vessels <100 μm in diameter. Furthermore, this vascular phenotype was markedly exaggerated by chronic hyperoxia. We also found that TGFBI expression was reduced in preterm lambs treated with NRS, consistent with delayed alveolarization observed in this group. Importantly, in preterm lambs maintained with the more injurious IMV strategy, TGFBI expression was abnormally increased along the thickened septal tips, similar to the abnormal accumulation of elastin and mesenchymal cell proliferation reported (14, 54). These studies suggest that both the correct amount and the correct location of TGFBI is required to optimally support vascular growth. Furthermore, these preclinical studies support recent clinical studies that offer additional evidence of the importance of TGFBI in the developing human lung. In a study of 50 twin pairs affected and unaffected with BPD, rare variants in *TGFBI* were associated with an increased risk for BPD (55). In a subsequent, larger study that used whole-exome sequencing in infants with extreme phenotypes of BPD, rare variants in *TGFBI* were again identified in affected but not unaffected subjects (56). Taken together, these studies provide compelling data to highlight the importance of TGFBI in promoting distal lung development and implicate a role for disrupted TGFBI signaling in the pathogenesis of BPD.

Our study has some limitations. Our proteomic analysis of the LCM used 2D-DIGE, protein spots were manually selected, and only the top 20 differentially expressed proteins were identified by mass spectroscopy. Thus, there are likely additional protein present in the LCM that serve to enhance NF-κB signaling and modify the proangiogenic phenotype of the PECs in addition to TGFBI. Newer methodologies that allow for a broader identification of differentially expressed proteins, including those with low abundance that may not have been identified with 2D-DIGE, represent important future studies. Although we were able to clearly show that TGFBI promotes PEC migration by binding to αvβ3 integrins, it is possible that TGFBI can also bind to addition integrins, resulting in distinct downstream effects. We performed transcriptomic profiling of primary PECs obtained from neonatal and adult mice to identify novel, TGFBI-mediated target genes. Although this approach allowed us to directly compare genes expressed by PECs at two distinct stages in development, there remains the possibility for confounding effects and change in phenotype as a result of cell culture. We attempted to mitigate these confounders by performing the analyses on two separate isolations of cells, and only including genes differentially expressed in both separate isolations. Nevertheless, future studies using single-cell RNA-seq in the WT and *Tgfbi* null mice could provide a more comprehensive assessment of all of the differentially expressed genes in both the EC and other lung cell types.

In summary, our data identify a paracrine mechanism by which myofibroblast expression of TGFBI promotes pulmonary angiogenesis through an αvβ3/NF-κB axis that increases CSF3-mediated NO production. Given the ability of TGFBI to bind extracellular matrix components highly expressed in the developing lung, local secretion of TGFBI by myofibroblasts may serve to create an angiogenic niche that promotes pulmonary vascular growth along the developing septa. Taken together, our studies identify a novel pathway allowing for myofibroblast–endothelial cross-talk, and we speculate that TGFBI dysregulation may contribute to the aberrant pulmonary angiogenesis observed in the setting of impaired alveolarization. ■

Author disclosures are available with the text of this article at www.atsjournals.org.

References

1. Bourbon J, Boucherat O, Chailley-Heu B, Delacourt C. Control mechanisms of lung alveolar development and their disorders in bronchopulmonary dysplasia. *Pediatr Res* 2005;57:38R–46R.
2. Jakkula M, Le Cras TD, Gebb S, Hirth KP, Tuder RM, Voelkel NF, *et al*. Inhibition of angiogenesis decreases alveolarization in the developing rat lung. *Am J Physiol Lung Cell Mol Physiol* 2000;279: L600–L607.
3. Thébaud B, Ladha F, Michelakis ED, Sawicka M, Thurston G, Eaton F, *et al*. Vascular endothelial growth factor gene therapy increases survival, promotes lung angiogenesis, and prevents alveolar damage in hyperoxia-induced lung injury: evidence that angiogenesis participates in alveolarization. *Circulation* 2005;112:2477–2486.
4. Islam JY, Keller RL, Aschner JL, Hartert TV, Moore PE. Understanding the short- and long-term respiratory outcomes of prematurity and bronchopulmonary dysplasia. *Am J Respir Crit Care Med* 2015;192: 134–156.

5. Baker CD, Alvira CM. Disrupted lung development and bronchopulmonary dysplasia: opportunities for lung repair and regeneration. *Curr Opin Pediatr* 2014;26:306–314.
6. Iosef C, Alastalo TP, Hou Y, Chen C, Adams ES, Lyu SC, *et al*. Inhibiting NF-κB in the developing lung disrupts angiogenesis and alveolarization. *Am J Physiol Lung Cell Mol Physiol* 2012;302: L1023–L1036.
7. De Palma M, Biziato D, Petrova TV. Microenvironmental regulation of tumour angiogenesis. *Nat Rev Cancer* 2017;17:457–474.
8. Boström H, Willetts K, Pekny M, Levéen P, Lindahl P, Hedstrand H, *et al*. PDGF-A signaling is a critical event in lung alveolar myofibroblast development and alveogenesis. *Cell* 1996;85:863–873.
9. Ahlfeld SK, Wang J, Gao Y, Snider P, Conway SJ. Initial suppression of transforming growth factor-β signaling and loss of TGFBI causes early alveolar structural defects resulting in bronchopulmonary dysplasia. *Am J Pathol* 2016;186:777–793.
10. Li ZW, Omori SA, Labuda T, Karin M, Rickert RC. IKKβ is required for peripheral B cell survival and proliferation. *J Immunol* 2003;170: 4630–4637.
11. Claxton S, Kostourou V, Jadeja S, Chambon P, Hodivala-Dilke K, Fruttiger M. Efficient, inducible Cre-recombinase activation in vascular endothelium. *Genesis* 2008;46:74–80.
12. Hilgendorff A, Reiss I, Ehrhardt H, Eickelberg O, Alvira CM. Chronic lung disease in the preterm infant: lessons learned from animal models. *Am J Respir Cell Mol Biol* 2014;50:233–245.
13. Hou Y, Liu M, Husted C, Chen C, Thiagarajan K, Johns JL, *et al*. Activation of the nuclear factor-κB pathway during postnatal lung inflammation preserves alveolarization by suppressing macrophage inflammatory protein-2. *Am J Physiol Lung Cell Mol Physiol* 2015; 309:L593–L604.
14. Reyburn B, Li M, Metcalfe DB, Kroll NJ, Alvord J, Wint A, *et al*. Nasal ventilation alters mesenchymal cell turnover and improves alveolarization in preterm lambs. *Am J Respir Crit Care Med* 2008; 178:407–418.
15. Albertine KH, Dahl MJ, Gonzales LW, Wang ZM, Metcalfe D, Hyde DM, *et al*. Chronic lung disease in preterm lambs: effect of daily vitamin A treatment on alveolarization. *Am J Physiol Lung Cell Mol Physiol* 2010;299:L59–L72.
16. Null DM, Alvord J, Leavitt W, Wint A, Dahl MJ, Presson AP, *et al*. High-frequency nasal ventilation for 21 d maintains gas exchange with lower respiratory pressures and promotes alveolarization in preterm lambs. *Pediatr Res* 2014;75:507–516.
17. Joss-Moore LA, Hagen-Lillevik SJ, Yost C, Jewell J, Wilkinson RD, Bowen S, *et al*. Alveolar formation is dysregulated by restricted nutrition but not excess sedation in preterm lambs managed by noninvasive support. *Pediatr Res* 2016;80:719–728.
18. Chu JE, Xia Y, Chin-Yee B, Goodale D, Croker AK, Allan AL. Lung-derived factors mediate breast cancer cell migration through CD44 receptor-ligand interactions in a novel ex vivo system for analysis of organ-specific soluble proteins. *Neoplasia* 2014;16: 180–191.
19. Park SW, Bae JS, Kim KS, Park SH, Lee BH, Choi JY, *et al*. Beta ig-h3 promotes renal proximal tubular epithelial cell adhesion, migration and proliferation through the interaction with alpha3beta1 integrin. *Exp Mol Med* 2004;36:211–219.
20. Iosef C, Liu M, Ying L, Rao SP, Concepcion KR, Chan WK, *et al*. Distinct roles for IκB kinases alpha and beta in regulating pulmonary endothelial angiogenic function during late lung development. *J Cell Mol Med* 2018;22:4410–4422.
21. Räthel TR, Leikert J JRF, Vollmar AM, Dirsch VM. Application of 4,5-diaminofluorescein to reliably measure nitric oxide released from endothelial cells in vitro. *Biol Proced Online* 2003;5: 136–142.
22. Guo M, Du Y, Gokey JJ, Ray S, Bell SM, Adam M, *et al*. Single cell RNA analysis identifies cellular heterogeneity and adaptive responses of the lung at birth. *Nat Commun* 2019;10:37.
23. Pierce JW, Schoenleber R, Jesmok G, Best J, Moore SA, Collins T, *et al*. Novel inhibitors of cytokine-induced IkappaBalpha phosphorylation and endothelial cell adhesion molecule expression show anti-inflammatory effects in vivo. *J Biol Chem* 1997;272: 21096–21103.
24. Son HN, Nam JO, Kim S, Kim IS. Multiple FAS1 domains and the RGD motif of TGFBI act cooperatively to bind αvβ3 integrin, leading to anti-angiogenic and anti-tumor effects. *Biochim Biophys Acta* 2013; 1833:2378–2388.
25. Brooks PC, Clark RA, Cheresh DA. Requirement of vascular integrin alpha v beta 3 for angiogenesis. *Science* 1994;264:569–571.
26. Scatena M, Almeida M, Chaisson ML, Fausto N, Nicosia RF, Giachelli CM. NF-kappaB mediates alphavbeta3 integrin-induced endothelial cell survival. *J Cell Biol* 1998;141:1083–1093.
27. Bhullar IS, Li YS, Miao H, Zandi E, Kim M, Shyy JY, *et al*. Fluid shear stress activation of IkappaB kinase is integrin-dependent. *J Biol Chem* 1998;273:30544–30549.
28. Ueda K, Takano H, Hasegawa H, Niitsuma Y, Qin Y, Ohtsuka M, *et al*. Granulocyte colony stimulating factor directly inhibits myocardial ischemia-reperfusion injury through Akt-endothelial NO synthase pathway. *Arterioscler Thromb Vasc Biol* 2006;26: e108–e113.
29. Roberts RJ, Weesner KM, Bucher JR. Oxygen-induced alterations in lung vascular development in the newborn rat. *Pediatr Res* 1983;17: 368–375.
30. Bhatt AJ, Pryhuber GS, Huyck H, Watkins RH, Metlay LA, Maniscalco WM. Disrupted pulmonary vasculature and decreased vascular endothelial growth factor, Flt-1, and TIE-2 in human infants dying with bronchopulmonary dysplasia. *Am J Respir Crit Care Med* 2001; 164:1971–1980.
31. Billings PC, Whitbeck JC, Adams CS, Abrams WR, Cohen AJ, Engelsberg BN, *et al*. The transforming growth factor-beta-inducible matrix protein (beta)ig-h3 interacts with fibronectin. *J Biol Chem* 2002;277:28003–28009.
32. Hanssen E, Reinboth B, Gibson MA. Covalent and non-covalent interactions of betaig-h3 with collagen VI: beta ig-h3 is covalently attached to the amino-terminal region of collagen VI in tissue microfibrils. *J Biol Chem* 2003;278:24334–24341.
33. Bae JS, Lee SH, Kim JE, Choi JY, Park RW, Yong Park J, *et al*. Betaig-h3 supports keratinocyte adhesion, migration, and proliferation through alpha3beta1 integrin. *Biochem Biophys Res Commun* 2002; 294:940–948.
34. Kim JE, Jeong HW, Nam JO, Lee BH, Choi JY, Park RW, *et al*. Identification of motifs in the fasciclin domains of the transforming growth factor-beta-induced matrix protein betaig-h3 that interact with the alphavbeta5 integrin. *J Biol Chem* 2002;277:46159–46165.
35. Nam JO, Kim JE, Jeong HW, Lee SJ, Lee BH, Choi JY, *et al*. Identification of the alphavbeta3 integrin-interacting motif of betaig-h3 and its anti-angiogenic effect. *J Biol Chem* 2003;278: 25902–25909.
36. Schwanekamp JA, Lorts A, Sargent MA, York AJ, Grimes KM, Fischesser DM, *et al*. TGFBI functions similar to periostin but is uniquely dispensable during cardiac injury. *PLoS One* 2017;12: e0181945.
37. Billings PC, Herrick DJ, Howard PS, Kucich U, Engelsberg BN, Rosenbloom J. Expression of betaig-h3 by human bronchial smooth muscle cells: localization to the extracellular matrix and nucleus. *Am J Respir Cell Mol Biol* 2000;22:352–359.
38. Heine UI, Munoz EF, Flanders KC, Roberts AB, Sporn MB. Colocalization of TGF-beta 1 and collagen I and III, fibronectin and glycosaminoglycans during lung branching morphogenesis. *Development* 1990;109:29–36.
39. Shull MM, Ormsby I, Kier AB, Pawlowski S, Diebold RJ, Yin M, *et al*. Targeted disruption of the mouse transforming growth factor-beta 1 gene results in multifocal inflammatory disease. *Nature* 1992;359: 693–699.
40. Kaartinen V, Voncken JW, Shuler C, Warburton D, Bu D, Heisterkamp N, *et al*. Abnormal lung development and cleft palate in mice lacking TGF-beta 3 indicates defects of epithelial-mesenchymal interaction. *Nat Genet* 1995;11:415–421.
41. Chen H, Sun J, Buckley S, Chen C, Warburton D, Wang XF, *et al*. Abnormal mouse lung alveolarization caused by Smad3 deficiency is a developmental antecedent of centrilobular emphysema. *Am J Physiol Lung Cell Mol Physiol* 2005;288: L683–L691.

42. Kim JE, Kim SJ, Lee BH, Park RW, Kim KS, Kim IS. Identification of motifs for cell adhesion within the repeated domains of transforming growth factor-beta-induced gene, betaig-h3. *J Biol Chem* 2000;275: 30907–30915.
43. Leavesley DI, Schwartz MA, Rosenfeld M, Cheresh DA. Integrin beta 1- and beta 3-mediated endothelial cell migration is triggered through distinct signaling mechanisms. *J Cell Biol* 1993;121: 163–170.
44. Brooks PC, Montgomery AM, Rosenfeld M, Reisfeld RA, Hu T, Klier G, *et al*. Integrin alpha v beta 3 antagonists promote tumor regression by inducing apoptosis of angiogenic blood vessels. *Cell* 1994;79: 1157–1164.
45. Drake CJ, Cheresh DA, Little CD. An antagonist of integrin alpha v beta 3 prevents maturation of blood vessels during embryonic neovascularization. *J Cell Sci* 1995;108:2655–2661.
46. Malyankar UM, Scatena M, Suchland KL, Yun TJ, Clark EA, Giachelli CM. Osteoprotegerin is an alpha vbeta 3-induced, NF-kappa B-dependent survival factor for endothelial cells. *J Biol Chem* 2000; 275:20959–20962.
47. Dunn SM, Coles LS, Lang RK, Gerondakis S, Vadas MA, Shannon MF. Requirement for nuclear factor (NF)-kappa B p65 and NF-interleukin-6 binding elements in the tumor necrosis factor response region of the granulocyte colony-stimulating factor promoter. *Blood* 1994;83: 2469–2479.
48. Bussolino F, Wang JM, Defilippi P, Turrini F, Sanavio F, Edgell CJ, *et al*. Granulocyte- and granulocyte-macrophage-colony stimulating factors induce human endothelial cells to migrate and proliferate. *Nature* 1989;337:471–473.
49. Genís L, Gonzalo P, Tutor AS, Gálvez BG, Martínez-Ruiz A, Zaragoza C, *et al*. Functional interplay between endothelial nitric oxide synthase and membrane type 1 matrix metalloproteinase in migrating endothelial cells. *Blood* 2007;110:2916–2923.
50. Lee PC, Salyapongse AN, Bragdon GA, Shears LL II, Watkins SC, Edington HD, *et al*. Impaired wound healing and angiogenesis in eNOS-deficient mice. *Am J Physiol* 1999;277:H1600–H1608.
51. Zhao X, Lu X, Feng Q. Deficiency in endothelial nitric oxide synthase impairs myocardial angiogenesis. *Am J Physiol Heart Circ Physiol* 2002;283:H2371–H2378.
52. MacRitchie AN, Albertine KH, Sun J, Lei PS, Jensen SC, Freestone AA, *et al*. Reduced endothelial nitric oxide synthase in lungs of chronically ventilated preterm lambs. *Am J Physiol Lung Cell Mol Physiol* 2001;281:L1011–L1020.
53. Bland RD, Albertine KH, Carlton DP, MacRitchie AJ. Inhaled nitric oxide effects on lung structure and function in chronically ventilated preterm lambs. *Am J Respir Crit Care Med* 2005;172:899–906.
54. Albertine KH, Jones GP, Starcher BC, Bohnsack JF, Davis PL, Cho SC, *et al*. Chronic lung injury in preterm lambs: disordered respiratory tract development. *Am J Respir Crit Care Med* 1999;159:945–958.
55. Li J, Yu KH, Oehlert J, Jeliffe-Pawlowski LL, Gould JB, Stevenson DK, *et al*. Exome sequencing of neonatal blood spots and the identification of genes implicated in bronchopulmonary dysplasia. *Am J Respir Crit Care Med* 2015;192:589–596.
56. Hamvas A, Feng R, Bi Y, Wang F, Bhattacharya S, Mereness J, *et al*.; PROP Investigators. Exome sequencing identifies gene variants and networks associated with extreme respiratory outcomes following preterm birth. *BMC Genet* 2018;19:94.